Isothermal and Cyclic Oxidation of MoAlB in Air from 1100°C to 1400°C

Sankalp Kota,[a,*,z] Eugenio Zapata-Solvas,[b] Yexiao Chen,[c] Miladin Radovic,[c] William E. Lee,[b] and Michel W. Barsoum[a,z]

[a]*Department of Materials Science & Engineering, Drexel University, Philadelphia, Pennsylvania 19104, USA*
[b]*Centre for Nuclear Engineering & Department of Materials, Imperial College London, SW7 2AZ, United Kingdom*
[c]*Department of Materials Science & Engineering, Texas A&M University, College Station, Texas 77843, USA*

Like many FeCrAl-based alloys, and some MAX phases, the atomically laminated boride, MoAlB, forms slow-growing, adherent Al_2O_3 scales when heated in air to 1350°C. Herein the oxidation of MoAlB ceramics in air was studied in the 1100–1400°C temperature range for up to 200 h. At 1400°C, the oxide scale was heavily cracked and spalled. At 1100°C, and up to 20 h, mass loss was recorded. At 1300°C and 1350°C, subparabolic, approximately cubic kinetics were observed, as a result of growth and coarsening of the Al_2O_3 grains in the oxide scale. At 1200°C, the weight gain kinetics were nearly linear, while the oxide thickening kinetics were approximately cubic likely due to cubic growth of Al_2O_3 and concurrent volatility of constituents in the oxide scale. The cyclic oxidation resistance was also good for up to 125, 1-hour, cycles at 1200°C. Analysis of grain coarsening and scale thickening kinetics suggest that oxygen grain boundary diffusivity is the rate controlling mechanism for the growth of Al_2O_3 scales at 1300°C and 1350°C. Dimensional changes at samples' corners after long oxidation at T > 1200°C may limit the maximum operational temperature of MoAlB.

 [DOI: 10.1149/2.1891713jes]

Manuscript submitted August 28, 2017; revised manuscript received October 11, 2017. Published November 10, 2017.

For oxidation resistance at temperatures exceeding 1000°C, materials that form protective alumina, Al_2O_3, scales are especially useful for long service and offer several advantages over chromia and silica formers. Notable examples include FeCrAl-based alloys (e.g. Hoskins 875 and PM2000)[1,2] and some Al-containing MAX phases (e.g. Ti_2AlC,[3–6] Cr_2AlC,[7–10] and Ti_3AlC_2)[11–13] that form well adhering, protective Al_2O_3 scales and follow approximately cubic oxidation kinetics up to 1400°C. Smialek et al. showed recently that diffusion through the grain boundaries of the coarsening Al_2O_3 grains in these scales is the rate controlling mechanism and leads to cubic kinetics for all the aforementioned materials.[14,15] In Ti_2AlC and Ti_3AlC_2, well-matched thermal expansion coefficients with Al_2O_3 generate low thermal stresses at the oxide/metal interface, rendering them effective even after a thousand hours of cyclic[16] and isothermal exposures,[13] and also under the high air flux environment of high pressure burner rigs.[17]

Recently, we reported on the synthesis and properties of another atomically laminated, Al_2O_3-forming compound, MoAlB, that has a MAX-like layered structure consisting of a Mo-B slabs, interleaved with two atomic layers of Al.[18–20] Similar to the aforementioned MAX phases, isothermal oxidation in air led to formation of oxide scales containing primarily α-Al_2O_3 up to 1400°C. The growth of the oxide scale thickness with time was found to follow approximately cubic kinetics at 1100°C and 1300°C. The scale was found to be well-adhered even after 200 h at 1300°C, which was attributed to the closely matched thermal expansion coefficients of MoAlB (9.5×10^{-6} K^{-1})[20] and Al_2O_3 (8.5×10^{-6} K^{-1}).[21] More recently, we showed that MoAlB incongruently melts in inert atmospheres at approximately 1435°C, but maintains high, and roughly temperature independent thermal conductivity values (>25 W/m/K) and high Young's moduli (319 GPa at 1200°C) up to the melting point.[22] Together, these properties bode well for its application at high temperatures in ambient air.

Using thermogravimetric analysis (TGA) and differential scanning calorimetry (DSC) on MoAlB powders, Okada et al.[23] showed that rapid mass gains and a corresponding exotherm were observed starting at approximately 700°C up to 900°C, that they associated with the formation of crystalline α-MoO_3, $Al_5(BO_3)O_6$, $Al_{18}B_4O_{33}$, and possibly amorphous B_2O_3. Above 900°C, rapid weight loss was observed until 1200°C.[23]

The only study to date on the oxidation kinetics of bulk MoAlB was not too detailed and was limited to 1100°C and 1300°C.[20] In this work, we revisit the oxidation behavior of MoAlB in more detail by carrying out oxidation studies in air over a wider temperature range (1100–1400°C) for up to 200 h in an attempt to better understand the oxidation kinetics, characterize the scale microstructure, and elucidate the oxidation mechanisms. We also compare our results to other Al_2O_3-forming materials. The kinetics of oxide scale thickening and mass change as a function of temperature are measured to elucidate both transient and steady state oxidation processes.

Experimental

Synthesis.—Molybdenum monoboride (MoB, Alfa Aesar, 99%, <38 μm) and aluminum (Al, Alfa Aesar, 99.5%) powders were combined in a molar ratio of 1.0 to 1.3 and mixed in a polyethylene jar using zirconia milling balls for 48 h. The mixed powders were precompacted at 30 MPa and placed into a boron nitride-coated graphite die. The die was placed in a graphite element heated hot press, HP, and heated under a mechanical vacuum (<20 Pa) at a rate of 300°C/h, to a peak temperature of 1200°C and a load corresponding to a stress of 25 MPa. This temperature and pressure were maintained for 5 h before cooling the HP naturally. The HPed samples' surfaces were ground with coarse diamond pads to remove graphite and boron nitride residue on the surface before further preparation for oxidation testing (see details below). The samples were fully dense (6.4 g/cm^3) and contained predominantly MoAlB, with 6 ± 3 vol.% Al_3Mo, Al_8Mo_3 and other Al-rich intermetallics, as well as <2 vol.% Al_2O_3 impurities.[22]

MoAlB powders were also prepared for oxidation testing, which were synthesized by cold-pressing the aforementioned mixture and heating it under dynamic vacuum in the hot press at 1000°C for 5 h without applied pressure. The resulting porous compact was ground into powders using a drill press equipped with a TiN-coated milling bit and sieved to a particle size less than 20 μm before further testing.

Oxidation testing.—The bulk MoAlB samples were electro-discharge machined into bars ($3 \times 4 \times 8$ mm^3). The bars were then progressively ground with SiC papers to 800 grit, cleaned with ethanol, and air dried. For isothermal testing of the bulk samples, the

*Electrochemical Society Student Member.
[z]E-mail: barsoumw@drexel.edu; ssk63@drexel.edu

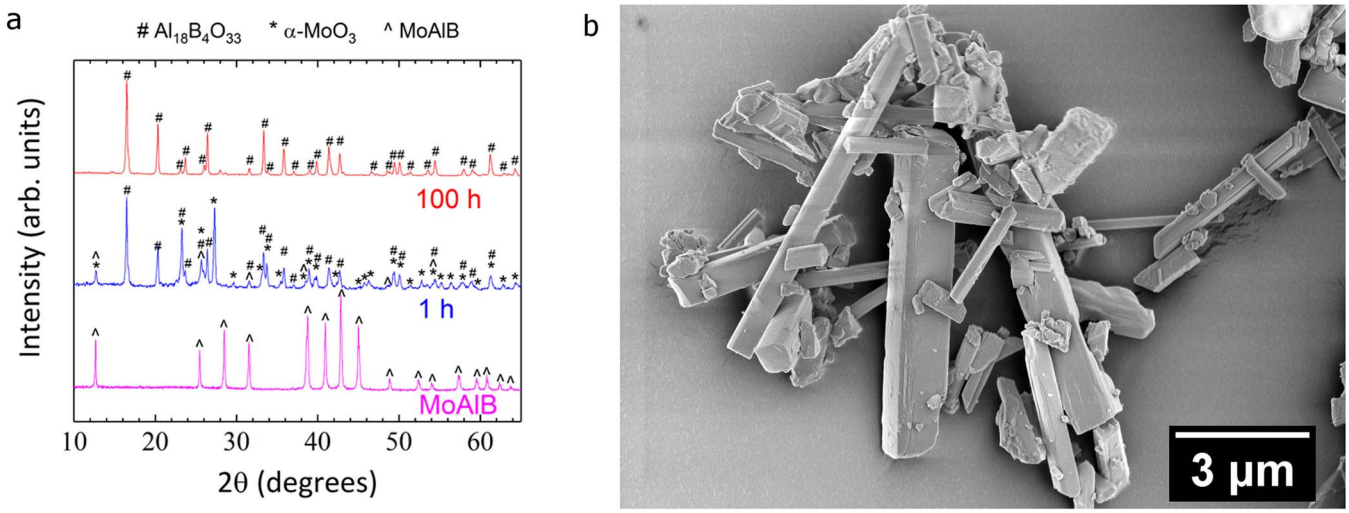

Figure 1. (a) XRD patterns of reaction product obtained from heating MoAlB powders in air at 1100°C for 1 h (bottom) and 100 h (top), and (b) micrograph of the reaction products after 100 h.

bars were heated in ambient air in a box furnace at a rate of 10°C/min, and held at peak temperature for up to 200 h at 1100°C, 1200°C, 1300°C, and 1350°C and up to 50 h at 1400°C, before cooling them at 10°C/min. Thus, for isothermal testing, a separate sample was used for each time/temperature condition. Samples were also heated at 10°C/min to 1100°C, 1200°C, 1300°C, and 1350°C, under dry, flowing air (20 mL/min) in a thermogravimetric analyzer (TGA, Netzsch STA 449F1), and held at the peak temperatures for 20 h, before cooling at the same rate.

For cyclic oxidation testing, three samples were heated and cooled together in ambient air in a box furnace, at a rate of 10°C/min, between 200°C to 1200°C and held at 1200°C for 1 h during each cycle. The samples were weighed intermittently before being placed back in the furnace for further thermal cycling. The total number of cycles was 125.

Oxidation of powders was conducted by placing several grams of MoAlB in an Al_2O_3 crucible that was heated in a box furnace at 10°C/min in ambient air to 1100°C and held at that temperature for 1 h or 100 h.

Characterization.—X-ray diffraction, XRD, was performed using a powder diffractometer (Rigaku SmartLab or Panalytical or Bruker AXS) using Cu-Kα_1 radiation. Scanning electron microscopy, SEM, and energy dispersive X-ray spectroscopy, EDS, were performed with a Zeiss Supra 50VP FESEM or Quanta 600 FESEM equipped with Oxford Inca X-sight EDS system. Fractured cross-sections were obtained by cutting the oxidized samples most of the way through their width using a low speed saw equipped with a diamond wheel and then fracturing it manually. Polished cross-sections were obtained by mounting the oxidized samples in epoxy and wet grinding them progressively from 240 grit to 1200 grit SiC paper. Oxide scale thicknesses were measured from micrographs of the polished cross-sections using ImageJ software, with each data point being the arithmetic mean and standard deviation of 25 measurements. The grain size in the oxide scale was estimated from micrographs of the samples' fractured cross-sections.

Results

Powder oxidation.—Figure 1a shows the XRD patterns of the starting MoAlB powders and those obtained after 1 h and 100 h of isothermal oxidation in ambient air. A mixture of α-MoO_3 (JCPDS #05-0508, space group *Pbnm*), $Al_{18}B_4O_{33}$ (space group $Cmc2_1$),[24] and unreacted MoAlB is present after 1 h. When heated for 100 h, however, only $Al_{18}B_4O_{33}$ is detected. Figure 1b shows the plate- and rod-like $Al_{18}B_4O_{33}$ phase formed after 100 h at 1100°C. Unlike Okada's study, $Al_5(BO_3)O_6$ was not detected by XRD.[23]

Isothermal oxidation of bulk MoAlB.—*Oxidation kinetics.*—The mass gains per unit area, ΔW/A, as a function of time, t, when bulk MoAlB samples were oxidized in ambient air at 1200, 1300, and 1350°C are shown in Fig. 2a. The mass gain (typically <0.003 kg/m^2 at all T) that occurred during heating to the desired temperature was accounted for by subtracting the mass gained from samples heated at the same rate to the desired temperatures with no subsequent isothermal holding time. At 1200°C, the mass increased steadily, without strong signs of asymptotic behavior. On the other hand, the mass increased rapidly within the first 5 h at 1300°C and 1350°C, after which the oxidation rates slow down significantly. The same trends were observed in samples oxidized in the TGA under flowing air in the 1200–1350°C range (Fig. 3a), but slightly higher mass gains were found compared to oxidation in static, ambient air at the end of 20 h. At 1100°C in the TGA, a gradual mass loss over 20 h resulted in a net mass loss of 0.006 kg/m^2 (Fig. 3a). However, a net mass gain was measured after 200 h of isothermal oxidation at 1100°C in air (Fig. 2a).

The normalized ΔW/A results were analyzed assuming parabolic, cubic or power law kinetics given, respectively, by the following relationships,

$$\left(\frac{\Delta W}{A}\right)^2 = k_{p,w}t \quad [1]$$

$$\left(\frac{\Delta W}{A}\right)^3 = k_{c,w}t \quad [2]$$

$$\frac{\Delta W}{A} = K't^n \quad [3]$$

where $k_{p,w}$, $k_{c,w}$ and K' are, respectively, the parabolic, cubic and power law constants; n is the power law exponent. The resulting rate constants, n values, and R^2 values are summarized in Table I.

Table I reveals that:

i. At 1300°C and 1350°C, the cubic rate law gave a slightly higher correlation coefficient than the parabolic rate law. The n values at 1300°C and 1350°C are 0.38 and 0.39, respectively, confirming the appropriateness of assuming cubic kinetics (n = 0.33) at these temperatures.
ii. At 1200°C, the same procedure led to n = 0.82. In other words, the kinetics are closer to linear than parabolic or cubic.

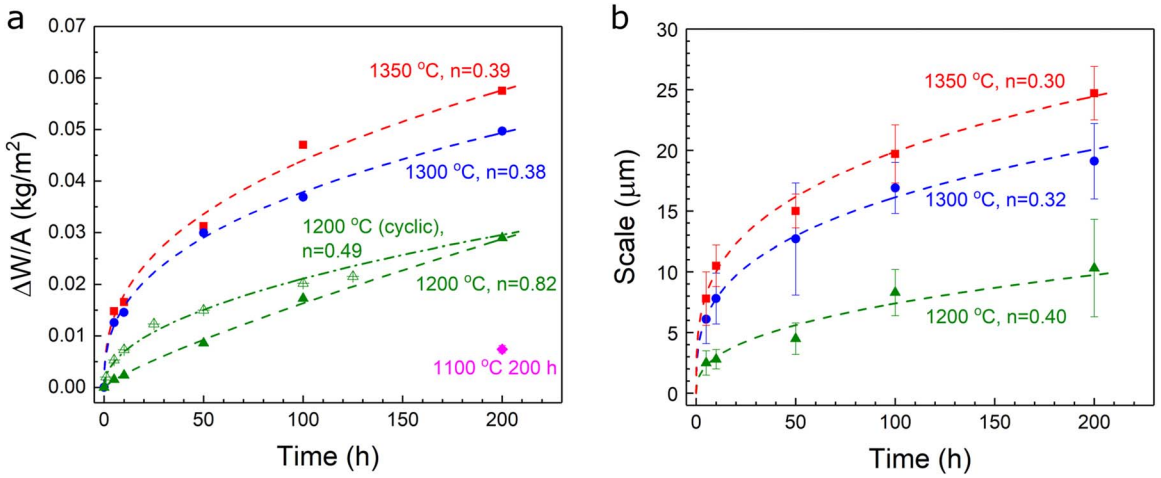

Figure 2. (a) Mass gain per unit surface area and (b) scale thickness, as a function of isothermal oxidation time for bulk MoAlB samples. The thickness and error bars in 2b represent the average and standard deviation of 25 independent measurements on each sample. The dashed lines show the modelled kinetics based on fitting to a power law similar to Eq. 3, with the indicated scale growth exponent shown in each case.

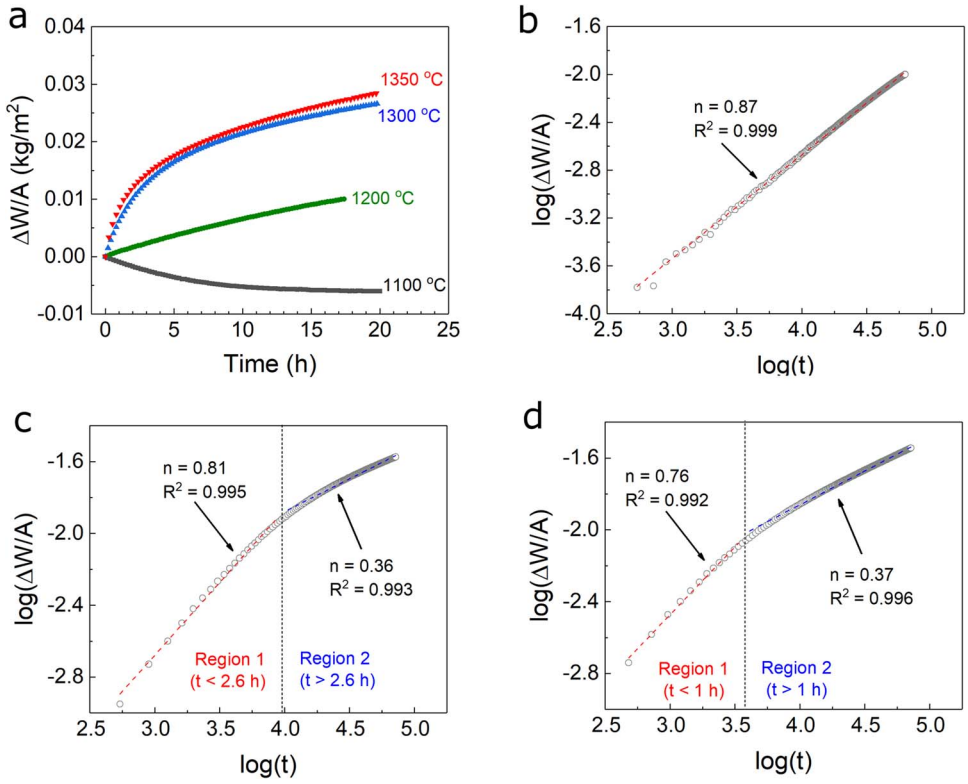

Figure 3. (a) Mass change per unit area for bulk MoAlB samples measured in TGA under flowing dry air, and log(ΔW/A) vs. log(t) plots at (b) 1200°C, (c) 1300°C, and (d) 1350°C.

Table I. Mass gain kinetic parameters and linear correlation coefficients derived by fitting experimental data to Eqs. 1–3 for oxidation testing isothermally in ambient air a box furnace (static), isothermally under flowing air (TGA), and interrupted cyclic tests (cyclic).

	Cubic		Parabolic		Linear		Power Law	
T (°C)	$K_{c,w}$ ($kg^3m^{-6}s^{-1}$)	R^2	$K_{p,w}$ ($kg^2m^{-4}s^{-1}$)	R^2	$K_{l,w}$ ($kgm^{-2}s^{-1}$)	R^2	n	R^2
1350 (static)	2.75×10^{-10}	0.98792	4.55×10^{-9}	0.97461	-	-	0.389	0.98516
1350 (TGA)	3.32×10^{-10}	0.99989	1.07×10^{-8}	0.98117	-	-	See Fig. 3d	
1300 (static)	1.71×10^{-10}	0.99226	3.27×10^{-9}	0.99110	-	-	0.383	0.99344
1300 (TGA)	2.78×10^{-10}	0.99754	9.67×10^{-9}	0.96908	-	-	See Fig. 3c	
1200 (static)	3.42×10^{-11}	0.90918	1.20×10^{-9}	0.97040	3.95×10^{-8}	0.99223	0.817	0.99739
1200 (TGA)	1.60×10^{-11}	0.90569	1.69×10^{-9}	0.97480	1.57×10^{-7}	0.99334	0.870	0.99953
1200 (cyclic)	2.29×10^{-11}	0.99625	1.03×10^{-9}	0.98491	-	-	0.486	0.98834

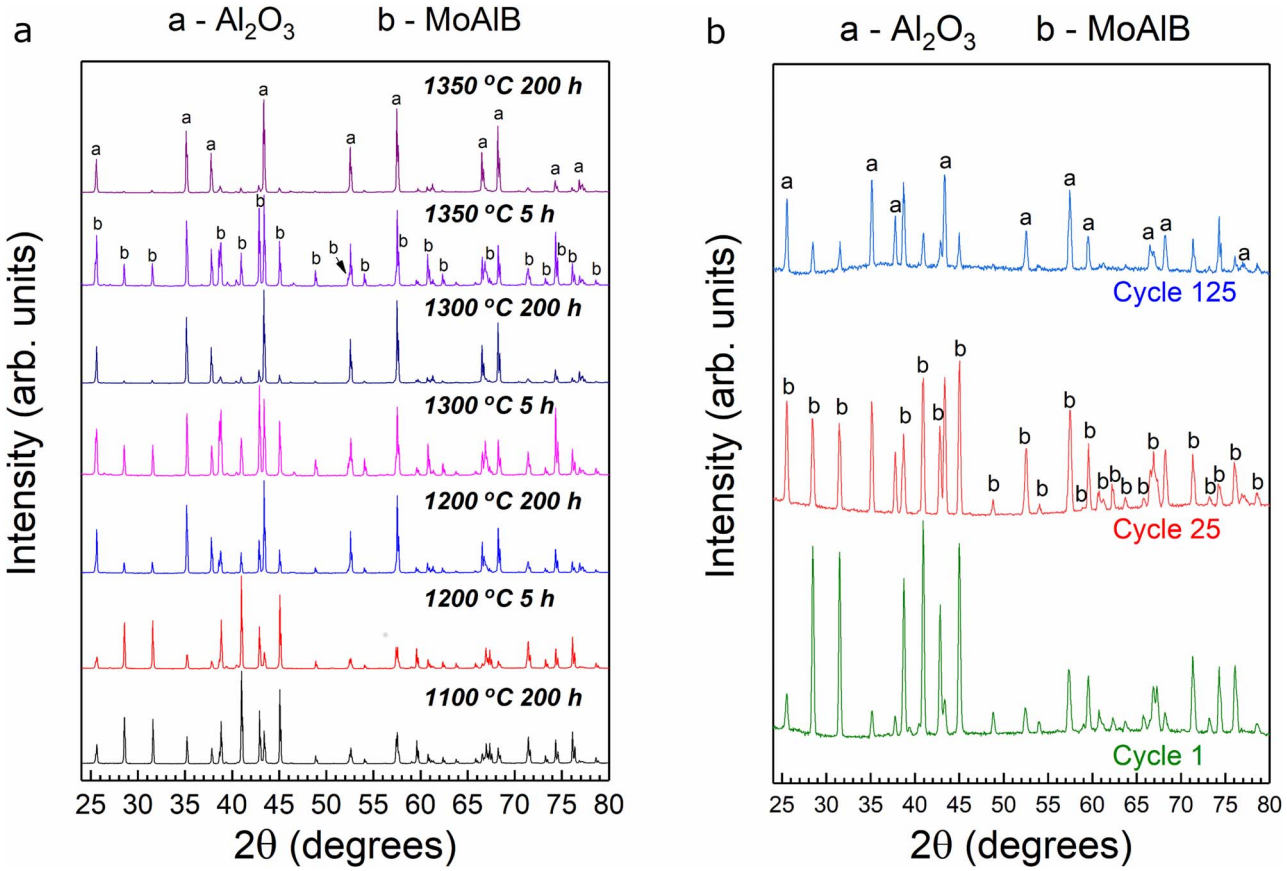

Figure 4. XRD of oxidized surfaces after (a) isothermal oxidation after various temperatures and times, and (b) cyclic oxidation at 1200°C after specified cycles.

A plot of log(ΔW/A) vs log(t) of the TGA results generally confirmed the above finding that the kinetics were close to linear at 1200°C, with n = 0.87 (Fig. 3b). On the other hand, the log-log plots at 1300°C and 1350°C revealed "knees" at times of ≈ 2.6 h and 1 h, respectively, which are marked with dotted lines as the points of highest curvature in Figs. 3c–3d. Before the knees, the slopes suggest nearly linear kinetics with n = 0.81 and 0.76, at 1300°C and 1350°C, respectively. After the knees, the kinetics are much closer to cubic with n = 0.36 at 1300°C and n = 0.37 at 1350°C. At 1100°C, unambiguous overall mass loss – at least for the first 20 h of oxidation – was recorded despite the fact that an alumina layer forms (Fig. 4a).

When the time dependencies of the scale thicknesses, Δx, are plotted (Fig. 2b), a different picture emerges. Again, the results were analyzed assuming cubic, parabolic and power laws. The results (Table II) indicate that:

i) At 1300°C and 1350°C, fitting to the cubic rate law give the highest correlation coefficients. The fact that the n values at these temperatures were 0.32 and 0.30, respectively, confirms this important finding.

ii) At 1200°C, the best fit is to cubic kinetics (R^2 = 0.972), is slightly better than parabolic (R^2 = 0.967). Fitting this data to the power law yields an n of 0.4, which is indicative of subparabolic, approximately cubic kinetics.

Based on the totality of these results, it is reasonable to conclude that the oxidation kinetics are approximately cubic at 1300°C and 1350°C. The situation at 1200°C is more ambiguous for reasons discussed below. The dashed curves in Figure 2 are power law fits to the measured mass gain and scale thickness versus time data using the parameters for power law fits in Tables I and II. We did not analyze the oxidation kinetics at 1400°C because heavily cracked and spalling oxide scales formed at this temperature, and large weight gains (>0.22 kg/m^2) were observed.

Phase composition and morphology of the oxide scale.—XRD patterns of the samples' surfaces after 5 h and 200 h of isothermal oxidation in ambient air at various temperatures are shown in Fig. 4a. At all temperatures studied, the primary oxide formed is α-Al_2O_3. Not surprisingly, the (116) peak of α-Al_2O_3, at 2θ = 57.7°, increased in intensity with increasing oxidation times and temperatures. In all the

Table II. Scale thickening kinetic parameters and linear correlation coefficients derived by fitting experimental data to equations similar to Eqs. 1–3 in that ΔW/A is replaced by Δx for isothermal oxidation in ambient air a box furnace.

	Cubic		Parabolic		Linear		Power Law	
T (°C)	$K_{c,x}$ (m^{3}s^{-1})	R^2	$K_{p,x}$ (m^{2}s^{-1})	R^2	$K_{l,x}$ (m s^{-1})	R^2	n	R^2
1350	2.07×10^{-20}	0.998	7.67×10^{-16}	0.987	-	-	0.299	0.990
1300	9.87×10^{-21}	0.964	4.70×10^{-16}	0.928	-	-	0.316	0.995
1200	1.60×10^{-21}	0.972	1.49×10^{-16}	0.967	1.36×10^{-11}	0.950	0.398	0.950
1100 Ref. 20	7.07×10^{-23}	0.960	2.23×10^{-17}	0.957	-	-	0.4	0.96

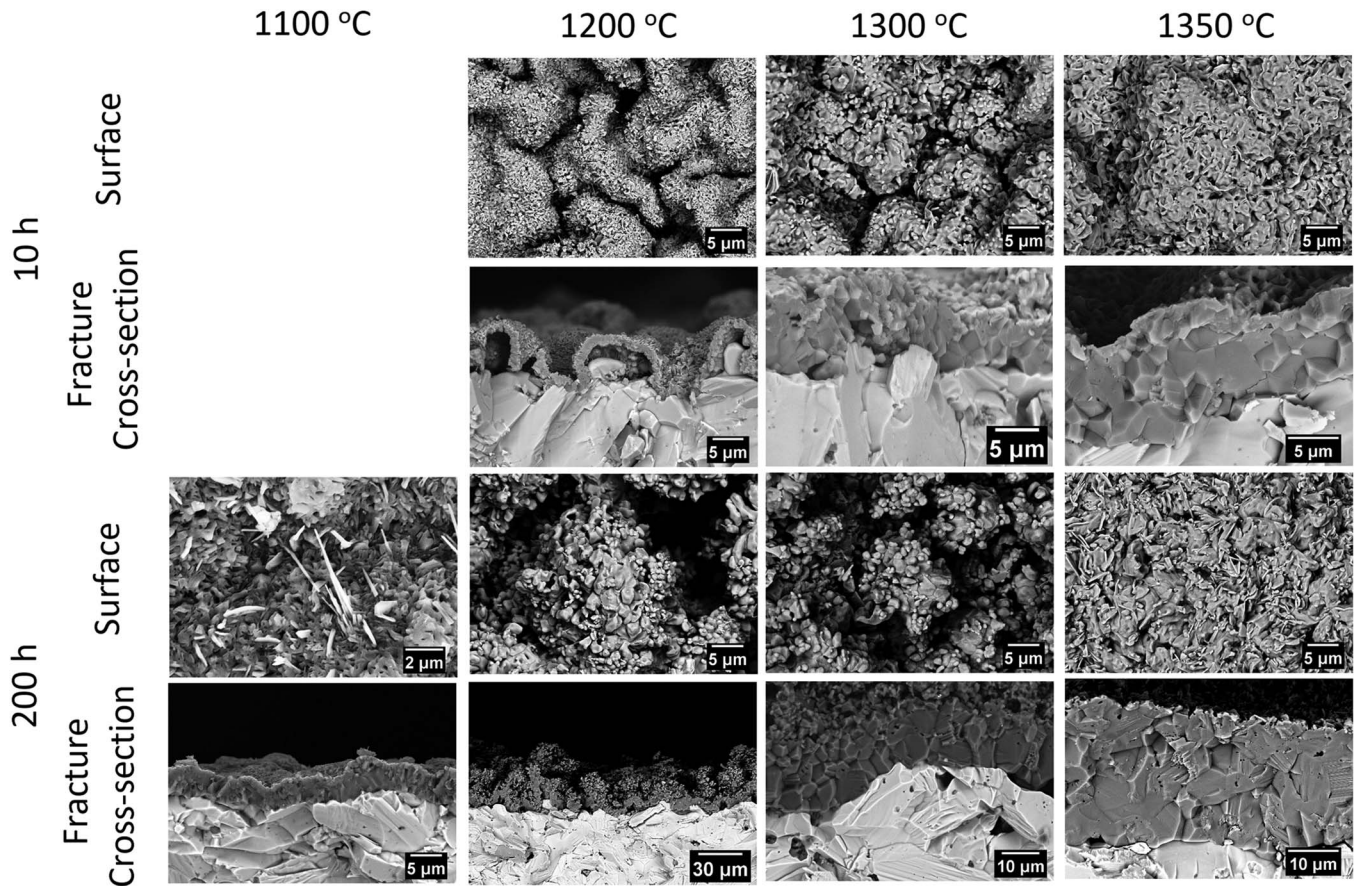

Figure 5. BSE micrographs of the outer scale surfaces and fractured cross-sections of the oxide/substrate interface after isothermal oxidation for 10 h and 200 h at temperatures indicated at the top.

XRD patterns of samples oxidized for 5 h, peaks corresponding to the underlying MoAlB can be identified, indirectly confirming that the oxide scales formed are quite thin. Though α-MoO_3 and $Al_{18}B_4O_{33}$ formed when MoAlB powders were oxidized (middle and top pattern in Fig. 1), no evidence of these phases was found in the XRD patterns of the oxidized bulk samples (Fig. 4a).

Figure 5 shows SEM backscattered electron (BSE) micrographs of the oxidized surfaces and fractured cross-sections of the oxide/substrate interfaces as a function of oxidation temperatures and oxidation times. The following observations are salient:

i. The oxide scale surfaces were comprised of mostly small, sub-micrometer sized grains. At 1200°C, particularly at short oxidation times, the oxide scales are undulating – with pores/cavities formed between the scale and substrate. Additional rod-like and/or plate-like particles are present on the oxide scale's surface after oxidation at both 1200°C and 1100°C (see first two columns of Fig. 5).
ii. After 10 h of oxidation at 1200°C, large voids (up to 10 µm in diameter) are present at the oxide/substrate interface. After t > 50 h at 1200°C, most of these voids appear to be filled with new grains (4th row of Fig. 5). The filling of voids with new grains leads to abnormally large apparent scale thicknesses in certain areas. These interfacial voids are present less frequently and generally only before 5 h at 1300°C and 1350°C.
iii. After oxidation at 1300°C and 1350°C, the oxide scale surfaces revealed the presence of only equiaxed grains, without the rod-like particles (see third and fourth columns of Fig. 5).
iv. EDS conducted on the oxide surfaces revealed that, regardless of temperature, the oxide surface contained predominantly Al and O in an atomic ratio 0.62-0.64, which is consistent with the XRD results showing the presence of α-Al_2O_3. Trace amounts of Mo were detected in some areas, in amounts less than 0.4 at.%.

Fractured cross-sections of oxidized samples show that the Al_2O_3 grains found at the oxide/MoAlB interface are also generally submicron sized even after 200 h at 1100°C and up to 50 h at 1200°C. After 200 h at 1200°C, the oxide grain size ranged from 1–3 µm. However, at 1300°C and 1350°C densely sintered Al_2O_3 grains are found at the interface, with grains on the order of 3 ± 1 µm after only 10 h, in stark contrast to the sub-micron sized grains found on the same samples' surfaces (first row of Fig. 5). Such differences between the oxide grain size at the metal/oxide interface versus the oxide scale surface have also been reported by Naumenko et al. in the Al_2O_3 scales formed on Y-doped FeCrAl.[25] As Fig. 5 shows qualitatively and Fig. 6a shows quantitatively, the Al_2O_3 grains near the interface coarsen steadily at these two temperatures, similar to other Al_2O_3 formers.[9,15] When fractured specimens were observed by SEM after oxidation at 1200°C, it was difficult to find clean oxide/metal interfaces to accurately determine grain sizes for every time/temperature condition. For this reason, grain size analysis at 1100 and 1200°C are not reported.

A representative EDS line scan across the oxide/MoAlB interface after oxidation for 5 h at 1300°C is shown in Fig. 7. Starting from 20 µm inside the MoAlB substrate, scanning toward the oxide/MoAlB interface shows the relative concentrations of Mo to Al to O to be constant, followed by an abrupt decrease in Mo content and a rapid spike in Al and O content as the scan passes into the oxide scale. The same is true at 1200°C and 1350°C (not shown). Note that the Mo content is greater than Al in the underlying MoAlB substrate due to the non-stoichiometry generally found in MoAlB.[19,22] Moreover, the good adhesion between the Al_2O_3 scales and the substrate, even in areas where pre-existing Al-rich intermetallics are present (see red arrows in Figs. 8b and 8c), suggest that they also contribute to Al_2O_3 formation.

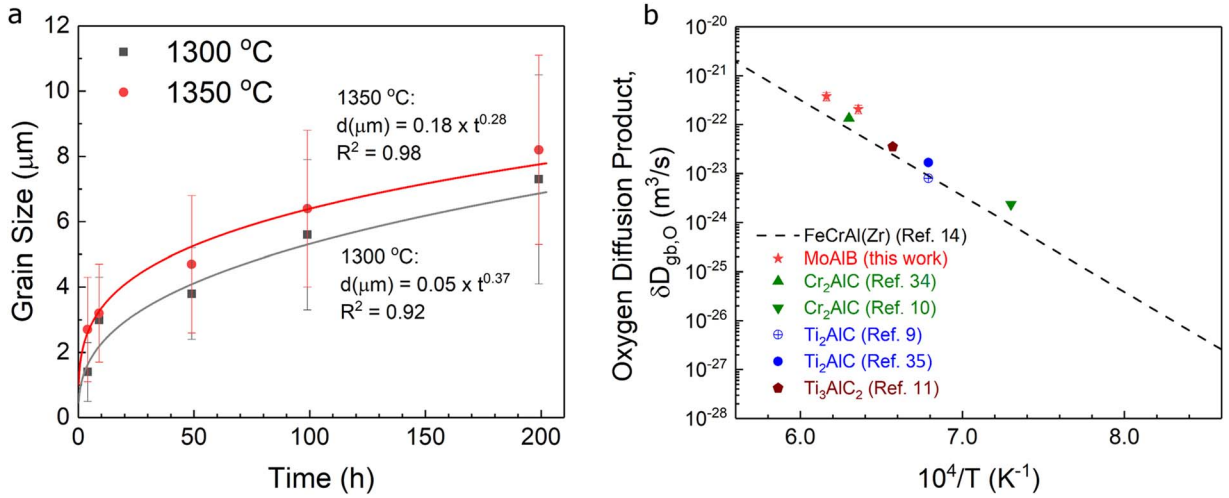

Figure 6. (a) Alumina grain size dependence on the oxidation time at 1300°C and 1350°C, and (b) oxygen grain boundary diffusivity of MoAlB calculated according to Eq. 10 compared to Hoskins 875 FeCrAl(Zr) alloy and select MAX phases adapted from Ref. 14, by analysis of data reported in Refs. 9–11, 15, 34, and 35.

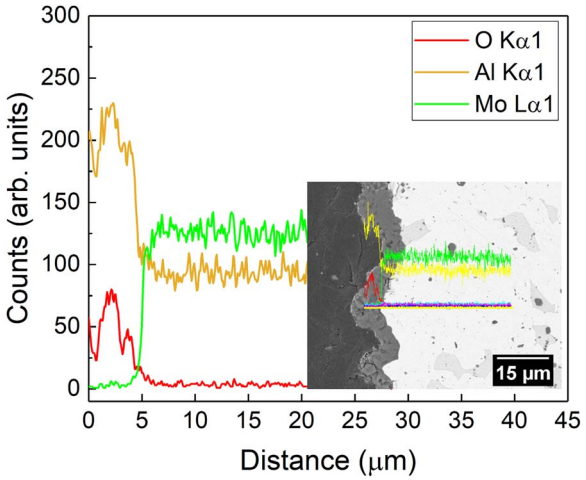

Figure 7. EDS line scan profiles across the MoAlB/oxide interface showing relative concentrations of Mo, Al, and O after 5 h of oxidation at 1300°C. Inset shows area where the EDS line profile was measured.

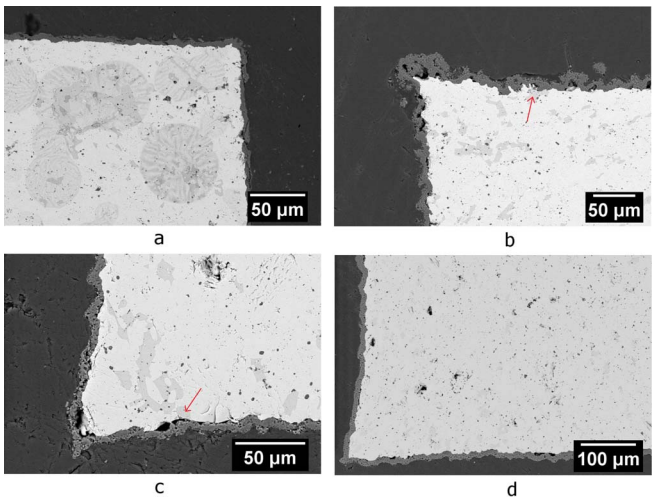

Figure 8. Sample corners after isothermal oxidation at (a) 1100°C 200 h, (b) 1200°C 200 h, (c) 1300°C 10 h, and (d) 1350°C 10 h. The red arrows show regions where the oxide scale formed on top of the intermetallic impurities.

Interestingly, Al_8Mo_3 and Al_4Mo intermetallics have been reported to form thin Al_2O_3 layers when Al_8Mo_3-coated Mo was oxidized in air.[26] Although 6 ± 3 vol. % of the intermetallics are present, their contribution to the mass gain is not known and not considered in this study.

A noticeable feature for most samples, especially after oxidation for 200 h at 1200°C and/or even short times (>10 h) at 1300°C or 1350°C is a clear distortion of the corners. After oxidation for 200 h at 1100°C, the edges at the corners are approximately normal to each other (Fig. 8a). In contrast, after 200 h at 1200°C (Fig. 8b), the sides are no longer perpendicular to each other. The same is true for the corners after oxidation for 10 h at 1300°C and 1350°C, shown, respectively, in Figs. 8c and 8d. Initially we assumed the reason was due to the samples' shrinkage. However, measurements of the samples' widths before, and after, oxidation showed that not to be the case. For example, the width of the sample, whose corners are shown in Fig. 8d, was 2.74 mm before oxidation and 2.8 mm after. Measurements on other samples, confirmed the same.

Cyclic oxidation at 1200°C.—The crossed, open green triangles in Fig. 2a show ΔW/A as a function of time up to 125 one-hour long cycles, assuming the total oxidation time is equal to only the time spent at 1200°C. Gradual mass gain is observed over the course of the 125 cycles, resulting in a small final mass gain of 2.15×10^{-2} kg/m^2. This mass gain is slightly higher than the 1.7×10^{-2} kg/m^2 measured after isothermal testing for 100 h. This is not surprising given the samples that are cycled spend more time at elevated temperatures (~40 minutes more per cycle at T > 1000°C) than those during the static oxidation tests at 1200°C. When the mass gain is fit to Eq. 3, a power law exponent of 0.49 is observed (Fig. 2a).

The XRD patterns of the sample surfaces after 1, 25 and 125 cycles is shown in Fig. 4b. After one cycle, it is dominated by peaks from the underlying MoAlB, but new peaks emerge at 35.1°, 37.8°, and 43.4° corresponding to Al_2O_3 after a larger number of cycles. With increasing cycles, the intensity of peaks assigned to Al_2O_3 relative to those of MoAlB increase reflecting the thickening of the Al_2O_3 scale.

Discussion

The overall conclusion of this work is that oxidation of MoAlB is more complex than previously envisioned, in which we simply assumed Al from MoAlB reacts with air to form a thin passivating Al_2O_3 layer following subparabolic, nearly cubic kinetics.[20] The results shown herein, especially the nearly linear kinetics at 1200°C (Figs. 2a and 3a–3b) and during the early stages at 1300°C and 1350°C

(Figs. 3c and 3d), as well as the lack of other phases at the substrate/oxide interface, all indicate that concomitant with the growth of the Al_2O_3 layers, a loss of both Mo and B could be occurring. That is, in addition to the inward diffusion of oxygen, there has to be an outward diffusion of Mo and B. In the remainder of this section, we present evidence for these conclusions.

a) *Propensity of Mo-oxides and B_2O_3 to evaporate/sublimate at elevated temperatures.* Based on the results shown in Fig. 1, it is reasonable to conclude that at short times the following reaction occurs:

$$18\ MoAlB + 54\ O_2 \rightarrow Al_{18}B_4O_{33(s)} + 18\ MoO_{3(s)} + 7B_2O_{3(s)} \quad [4]$$

The absence of Mo containing compounds in XRD after 100 h oxidation (Fig. 1a) implies that it simply evaporates or sublimates according to:

$$MoO_{3(s,l)} \rightarrow MoO_{3(g)} \quad [5]$$

This reaction is known to occur quite rapidly above 700°C when Mo is oxidized.[27,28] For example, Gulbransen et al. showed only net mass lost at all T > 700°C - with values of nearly 70–75 mg/cm^2 after just 8 min of oxidation at T ≥ 1100°C - when pure Mo rods were oxidized in oxygen due to the volatilization of MoO_3.[27] At 550°C, the same study showed that Mo metal oxidizes to readily form MoO_3 plate- and rod-shaped crystallites starting at 550°C, which then sublimate rapidly above 700°C.[27]

Similarly, the absence of B_2O_3 in the XRD patterns suggests that it is either amorphous and/or may have also evaporated after forming, according to

$$B_2O_{3(s)} \rightarrow B_2O_{3(g)} \quad [6]$$

Evaporation of B_2O_3 from oxide scales fromed on transition metal diborides at T > 1000°C is well-documented.[29,30]

If one assumes all the B_2O_3 and MoO_3 phases evaporate, then the overall oxidation reaction is:

$$18\ MoAlB + 54\ O_2 \rightarrow Al_{18}B_4O_{33(s)} + 18\ MoO_{3(g)} + 7\ B_2O_{3(g)} \quad [7]$$

Note that if B_2O_3 regions had been present in the oxide layers, there would have been regions that would have been denuded of Al and Mo (B cannot be accurately quantified in EDS). None were found, which strongly suggest that any B_2O_3 which formed during oxidation evaporated.

Moreover, given that α-MoO_3 is detected after the oxidation of MoAlB powders for 1 h (Fig. 1 and Eq. 4), it is reasonable to expect it when bulk MoAlB specimens are oxidized. Its absence thus suggests that it either does not form, or forms and evaporates at very short oxidation times. Gulbransen and Floquet et al. confirmed that in the 650–800°C range, MoO_3 volatilizes by sublimation as fast as it forms on Mo substrates.[27,28] It remains an open question whether it, as well as other Mo-oxides, is formed when bulk MoAlB is oxidized.

If Al were the only species being oxidized, its out-diffusion would eventually lead to the precipitation of phases rich in Mo and B below the oxide layer. The lack of such precipitates at the oxide/MoAlB interface indirectly suggests that Mo and B may diffuse outward as well. Alternatively, the lack Mo- and B- rich phases may simply suggest that the Al reservoir has not been sufficiently depleted to promote the formation of such phases. The latter possibility is believed to occur in the alumina-forming Fe-based alloys and MAX phases, in which the diffusion of Al is high enough to eliminate all concentration gradients. In other words, the entire sample becomes the reservoir. The layered nature of MoAlB suggests that to be the outcome here as well.

Lastly, in our previous work, we showed that the reaction:

$$\frac{1}{3}MoAlB \rightarrow \frac{1}{6}B_2O_3 + \frac{1}{3}MoO_3 + \frac{1}{6}Al_2O_3 \quad [8]$$

is predicted to have negative standard free energies of reaction, ΔG°, in the range of −461 to −420 kJ/mol O_2 in the 1100–1400°C temperature range studied herein.[22] We note, however, that these calculations were relatively simple and did not consider the formation of other Mo-oxides such as MoO_2 or oligomerized Mo-oxide species, which were reported in spectroscopic studies of oxide volatility during Mo metal oxidation.[31–33]

b) *Evidence for bubble formation and/or oxide buckling*: The porous, undulating nature of the oxide scale surfaces despite the presence of an apparently dense Al_2O_3 layer at the oxide/substrate interface may suggest gas evolution at some stage. This is best seen in the cross-sectional SEM micrograph of the sample oxidized at 1200°C for 10 h (second row in Fig. 5). The swelling noted above could reflect the effect of small pores. Another possibility is buckling of the oxide layer either at temperature or due to the generation of residual stresses during cooling (see below). In general, more work in needed to understand the origin of the buckling.

c) *Near linear kinetics in mass gain, but near cubic kinetics in scale thickening at 1200°C*: When the green curves in Figs. 2a and 2b, respectively, are compared it is clear that the increase in thickness of the Al_2O_3 layer is approximately cubic, whereas the mass gain is approximately linear.

d) In the sample heated to 1100°C for ≈ 20 h under flowing air in a TGA, a net small (0.2%) mass loss was recorded (see Fig. 3a). This observation presents direct evidence for mass loss.

Based on the totality of our results, it is reasonable to conclude that the overall oxidation reaction between 1200 and 1350°C in air is:

$$MoAlB + \left(3x + \frac{3y}{2} + \frac{3z}{2}\right)O_2 \rightarrow Mo_{1-x}Al_{1-y}B_{1-z} + \frac{y}{2}Al_2O_3 + x\,MoO_3\,(g) + \frac{z}{2}B_2O_3\,(g) \quad [9]$$

We can further conclude that the oxidation kinetics for the growth of the Al_2O_3 scale are subparabolic, and approximately cubic. To gain further insight into the rate controlling mechanism, we applied the approach of Smialek et al. to analyze our results for temperatures above 1200°C, at which continuous, protective oxide scales form.[14,15] That study demonstrated that the interfacial grain boundary diffusivity of oxygen through Al_2O_3 scales follows essentially the same temperature dependence as that of oxygen diffusion through high-purity, bulk polycrystalline Al_2O_3. By assuming grain boundary diffusion of oxygen dominates, and taking into account the coarsening of Al_2O_3 grains, a time-invariant constant Π_i proportional to the interfacial oxygen grain boundary diffusivity, $D_{gb,O,int}$, is given by:

$$\Pi_i = k_{p,i}G_i = 12\delta D_{gb,O,int} \quad [10]$$

where δ is the grain boundary width (assumed to be ~1 nm) and $k_{p,i}$ and G_i are the instantaneous parabolic rate constants and interfacial Al_2O_3 grain diameters at a given time. Using the scale thickening (Table II) and grain coarsening data (Fig. 6a) at 1300°C and 1350°C, $\delta D_{gb,O,int}$ values of 1.6×10^{-22} to 2.7×10^{-22} m^{3}s^{-1} at 1300°C and 3.1×10^{-22} to 4.6×10^{-22} m^{3}s^{-1} at 1350°C were obtained. These data points are shown on the Arrhenian plot of $\delta D_{gb,O,int}$ in Fig. 6b and agree well with those predicted in Ref. 14 for FeCrAl-based alloy Hoskins 875 and Al_2O_3-forming MAX phases, by analysis of data made available in previous studies.[3,9–11,34,35] Thus, it is likely that oxygen grain boundary diffusivity is also the rate controlling mechanism for the formation of Al_2O_3 scales on MoAlB.

As a further check of the correctness of assuming cubic kinetics controlled by the formation of α-Al_2O_3, we converted the k_x values in Table II to k_w by assuming the formation of a fully dense Al_2O_3, which has a density of 3950 kg/m^3. This was done by multiplying the former by $(3950\ kg/m^3 * 0.47)^3 = 6.4 \times 10^9\ kg^3/m^9$), where 0.47 is the mass fraction of O in α-Al_2O_3. Figure 9 shows the actual mass gains along with mass gains predicted by a k_w calculated from the conversion factor above at 1200°C (i.e. 1.02×10^{-11} kg^3/m^{6}s). Comparing the two shows that the measured mass gain is initially lower than that predicted by the formation of a dense alumina layer, but the former eventually overtakes the predicted mass gain. Repeating the procedure

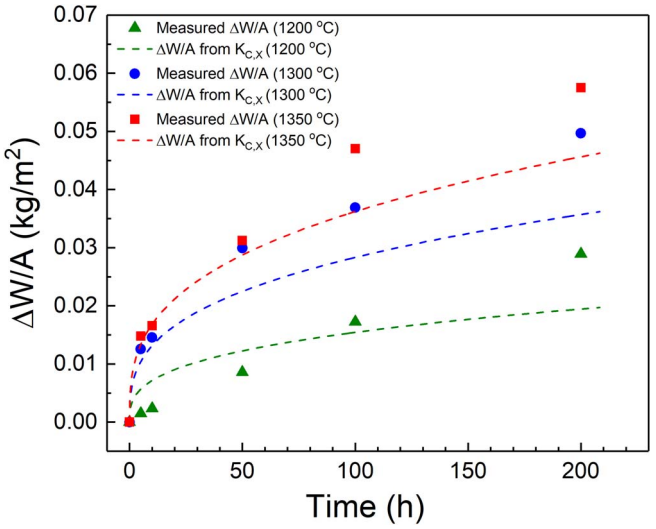

Figure 9. Mass gain predicted by thickness rate constants in Table II, assuming a fully dense Al_2O_3 scale is formed, compared to experimentally measured weight gains.

at 1300°C and 1350°C yield calculated cubic rate constants of 6.32×10^{-11} kg^3/m^6s and 1.32×10^{-10} kg^3/m^6s, respectively, which are both lower than the experimental values listed in Table I. One reason the experimentally measured mass gains are generally higher than those calculated from the k_x values could be our underestimation of the oxide thickness values. If the more porous outer oxide near the air/oxide surface is destroyed or buried during mounting and polishing, then the oxide thickness and thus k_x are underestimated. For example, in some cases, oxide scale thicknesses up to 30 μm were observed locally in fracture cross-sections after 200 h at 1200°C. When the same sample was mounted and polished, typical oxide thicknesses values were only 10 ± 4 μm. Note that, higher "true" $k_{p,I}$ values would increase the calculated $\delta D_{gb,O,int}$ values shown in Fig. 6b.

It is important to point out that the filling of the sub-scale pores, formed at shorter times with Al_2O_3 at longer times, confirms that oxygen diffuses through the Al_2O_3 scale. This is best seen by comparing the cross-sectional SEM micrograph of a sample oxidized at 1200°C after 10 h (second row in Fig. 5) and after 200 h (fourth row in Fig. 5).

During cyclic oxidation testing, the mass gain behavior is indicative of a well-adhering oxide scale resistant to spallation. Thus, the cyclic oxidation resistance at 1200°C is comparable to Ti_2AlC (2.3 mg/cm^2 after 125 cycles),[4,16] Ti_3AlC_2,[36] and some FeCrAl-based alloys.[2,37,38] The choice of assuming the total oxidation time to be equal to the time spent at 1200°C may have caused the differences between the kinetics observed under cyclic and isothermal conditions (compare the two green curves in Fig. 2a). Another reason for the discrepancy could be that the undulating oxide layer cracks without massive spallation resulting in a faster initial mass gain than the isothermal test at 1200°C. These comments notwithstanding, it is acknowledged that more work is needed to understand the small differences observed. We note that the reasons for the poor oxidation kinetics at 1200°C or their ramifications for exposures longer than 200 h are not yet well understood.

The residual thermal stresses in the oxide scales at room temperature can be estimated using the following relation:

$$\sigma_{ox} = -\frac{E_{ox}}{1-\nu_{ox}} \cdot \frac{(\alpha_{ox}-\alpha_s)\,\Delta T}{1+\frac{E_{ox}(1-\nu_s)}{E_s(1-\nu_{ox})}\frac{h_{ox}}{h_s}} \qquad [11]$$

where E is the elastic modulus, ν is the Poisson's ratio, h is thickness, α is the thermal expansion coefficient, and ΔT is the temperature difference upon cooling.[39,40] The subscripts "ox" and "s" indicate the properties for the oxide and underlying MoAlB substrate, respectively.

Using Eq. 11 and typical values of the physical properties for Al_2O_3 (E_{ox} = 400 GPa, ν_{ox} = 0.25, $\alpha_{ox} = 8.5 \times 10^{-6}$ K^{-1})[16,21] and those recently obtained values for MoAlB,[20,22] the residual thermal stresses from cycling are estimated to be compressive and on the order of 0.6 GPa. This value is only slightly higher than those found in the Al_2O_3 scales on Ti_2AlC[16] and NiO scales on Ni,[40] but lower than those reported for many metal alloys and intermetallics. Compressive stresses of this magnitude are large enough to cause substantial plastic deformation of Al_2O_3 scales at temperatures and stresses as low as 1050°C and 100 MPa, respectively.[41] Thus, the deformation of the scales may be a consequence of both cooling stresses due to thermal expansion mismatch, high temperature creep of the oxide scale, and possibly MoAlB's high-temperature deformation. These comments notwithstanding, we note in passing that the fact that at longer times, the voids are filled with smaller grains is consistent with a scenario where the deformation of the alumina layer occurs at temperature and not during cooling. More work is need to understand the deformation of the scales.

The results in this paper suggest some important practical considerations, which would likely limit the use of MoAlB components for long-term service in oxidizing environments. Namely, the dimensional changes – whose origin is unclear at this time – shown in Fig. 8 that occur after only 10 h of oxidation at T ≥ 1300°C could reduce its usefulness in some applications. This is in stark contrast to the MAX phase Ti_2AlC, which has been shown to maintain roughly perpendicular edges at the corners even after 2800 h at 1200°C.[9] The poor oxidation kinetics below this temperature may require pre-oxidation treatments to establish a dense well-adhered Al_2O_3 layer at the oxide/MoAlB interface, as observed after isothermal oxidation at 1300°C or above.

These comments notwithstanding, it is reasonable to assume that as the details of the oxidation mechanisms uncovered herein are better understood, their downside can be mitigated. This is but the second report on the oxidation of MoAlB, which remains the only transition metal boride that is oxidation resistant, and further studies are needed.

Conclusions

The isothermal oxidation of powder and bulk MoAlB in air from 1100°C to 1400°C for up to 200 h and cyclic oxidation at 1200°C for up to 125 h was investigated. At 1400°C, the oxide scale was heavily cracked and spalled. Although the kinetics of scale thickening are found to follow approximately cubic kinetics at all temperatures, the kinetics of mass gain are found to be more complicated. In particular, the mass gain kinetics at 1200°C are not cubic, which we ascribe to mass losses associated with volatilization of transient Mo and/or B oxides. In addition, the cyclic oxidation resistance of MoAlB at 1200°C for up to 125 1-h long cycles showed that the Al_2O_3 oxide scale is quite resistant to spallation.

Acknowledgments

This work we funded by the CMMI division of NSF (Grant numbers 1729335 and 1729350). E.Z.S and W.E.L. work was funded by EPSRC (EP/M018563/1; EP/M018768/1). Y. C. and M. R. acknowledge support from NSF through grant No. DMR-1410983 to Texas A&M University. We thank Dr. Guobing Ying (Drexel University) for help with sample preparations.

References

1. S. Dryepondt, J. Turan, D. Leonard, and B. A. Pint, *Oxid. Met.*, **87**, 215 (2017).
2. J. L. Smialek, J. A. Nesbitt, C. A. Barrett, and C. E. Lowell, *NASA/TM 2000–209769: Cyclic Oxidation Testing and Modelling: A NASA Lewis Perspective* (Cleveland, OH United States, 2000).
3. X. H. Wang and Y. C. Zhou, *Oxid. Met.*, **59**, 303 (2003).
4. M. Sundberg, G. Malmqvist, A. Magnusson, and T. El-Raghy, *Ceram. Int.*, **30**, 1899 (2004).
5. S. Basu, N. Obando, A. Gowdy, I. Karaman, and M. Radovic, *J. Electrochem. Soc.*, **159**, C90 (2012).

6. J. L. Smialek, *Oxid. Met.*, **83**, 351 (2015).
7. Z. J. Lin, M. S. Li, J. Y. Wang, and Y. C. Zhou, *Acta Mater*, **55**, 6182 (2007).
8. S. Li, X. Chen, Y. Zhou, and G. Song, *Ceram. Int.*, **39**, 2715 (2013).
9. D. J. Tallman, B. Anasori, and M. W. Barsoum, *Mater. Res. Lett.*, **1**, 115 (2013).
10. D. B. Lee and T. D. Nguyen, *J. Alloys Compd.*, **464**, 434 (2008).
11. X. Wang and Y. Zhou, *Corros. Sci.*, **45**, 891 (2003).
12. X. H. Wang, F. Z. Li, J. X. Chen, and Y. C. Zhou, *Corros. Sci.*, **58**, 95 (2012).
13. X. Li, L. Zheng, Y. Qian, J. Xu, and M. Li, *Corros. Sci.*, **104**, 112 (2016).
14. J. L. Smialek, *Corros. Sci.*, **91**, 281 (2015).
15. J. L. Smialek, N. S. Jacobson, B. Gleeson, D. B. Hovis, and A. H. Heuer, *NASA/TM-2013-217855: Oxygen Permeability and Grain-Boundary Diffusion Applied to Alumina Scales* (2013).
16. J. W. Byeon, J. Liu, M. Hopkins, W. Fischer, N. Garimella, K. B. Park, M. P. Brady, M. Radovic, T. El-Raghy, and Y. H. Sohn, *Oxid. Met.*, **68**, 97 (2007).
17. J. L. Smialek, *J. Eur. Ceram. Soc.*, **37**, 23 (2017).
18. W. Jeitschko, *Monatshefte Für Chemie Und Verwandte Teile Anderer Wissenschaften*, **97**, 1472 (1966).
19. M. Ade and H. Hillebrecht, *Inorg. Chem.*, **54**, 6122 (2015).
20. S. Kota, E. Zapata-Solvas, A. Ly, J. Lu, O. Elkassabany, A. Huon, W. E. Lee, L. Hultman, S. J. May, and M. W. Barsoum, *Sci. Rep.*, **6**, 26475 (2016).
21. E. R. Dobrovinskaya, L. A. Lytvynov, and V. Pishchik, in *Sapphire Mater. Manuf. Appl.*, 2009th ed. (Springer Science & Business Media, 2009), pp. 109.
22. S. Kota, M. Agne, E. Zapata-Solvas, O. Dezellus, D. Lopez, B. Gardiola, M. Radovic, and M. W. Barsoum, *Phys. Rev. B*, **95**, 144108 (2017).
23. S. Okada, *Trans. Kokushikan Univ. Fac. Eng.*, 7 (1998).
24. M. Ihara, K. Imai, J. Fukunaga, and N. Yoshida, *J. Ceram. Assoc. Japan*, **88**, 77 (1980).
25. D. Naumenko, B. Gleeson, E. Wessel, L. Singheiser, and W. J. Quadakkers, *Metall. Mater. Trans. A Phys. Metall. Mater. Sci.*, **38A**, 2974 (2007).
26. T. Maruyama, B. X. Fang, and K. Nagata, *J. Japan Inst. Met.*, **55**, 1222 (1991).
27. E. A. Gulbransen, K. F. Andrew, and F. A. Brassart, *J. Electrochem. Soc.*, **110**, 952 (1963).
28. N. Floquet, O. Bertrand, and J. J. Heizmann, *Oxid. Met.*, **37**, 253 (1992).
29. T. A. Parthasarathy, R. A. Rapp, M. Opeka, and R. J. Kerans, *Acta Mater*, **55**, 5999 (2007).
30. W. G. Fahrenholtz and G. E. Hilmas, *Int. Mater. Rev.*, **57**, 61 (2012).
31. J. B. Berkowitz-Mattuck, A. Büchler, J. L. Engelke, and S. N. Goldstein, *J. Chem. Phys.*, **39**, 2722 (1963).
32. J. Berkowitz, M. G. Inghram, and W. A. Chupka, *J. Chem. Phys.*, **26**, 842 (1957).
33. M. S. Samant, A. S. Kerkar, S. R. Bharadwaj, and S. R. Dharwadkar, *J. Alloys Compd.*, **187**, 373 (1992).
34. D. E. Hajas, M. To Baben, B. Hallstedt, R. Iskandar, J. Mayer, and J. M. Schneider, *Surf. Coatings Technol.*, **206**, 591 (2011).
35. G. M. Song, V. Schnabel, C. Kwakernaak, S. Van Der Zwaag, J. M. Schneider, and W. G. Sloof, *Mater. High Temp.*, **29**, 205 (2012).
36. X. K. Qian, X. D. He, Y. B. Li, Y. Sun, H. Li, and D. L. Xu, *Corros. Sci.*, **53**, 290 (2011).
37. C. E. Lowell and D. L. Deadmore, *Oxid. Met.*, **14**, 325 (1980).
38. M. Turker and T. A. Hughes, *Oxid. Met.*, **44**, 505 (1995).
39. G. D. Oxx, *Prod. Eng*, **29**, 61 (1958).
40. C. Liu, A.-M. Huntz, and J.-L. Lebrun, *Mater. Sci. Eng. A*, **160**, 113 (1993).
41. Y. Tamura, B. M. Moshtaghioun, E. Zapata-Solvas, D. Gomez-Garcia, A. D. Rodríguez, C. Cerecedo-Fernández, and V. Valcárcel-Juárez, *J. Eur. Ceram. Soc.*, (2017).